

Rethinking Context Aggregation in Natural Image Matting

Qinglin Liu¹, Shengping Zhang^{1*}, Quanling Meng¹, Ru Li¹, Bineng Zhong², Liqiang Nie¹
¹Harbin Institute of Technology ²Guangxi Normal University

Abstract

For natural image matting, context information plays a crucial role in estimating alpha mattes especially when it is challenging to distinguish foreground from its background. Existing deep learning-based methods exploit specifically designed context aggregation modules to refine encoder features. However, the effectiveness of these modules has not been thoroughly explored. In this paper, we conduct extensive experiments to reveal that the context aggregation modules are actually not as effective as expected. We also demonstrate that when learned on large image patches, basic encoder-decoder networks with a larger receptive field can effectively aggregate context to achieve better performance. Upon the above findings, we propose a simple yet effective matting network, named AEMatter, which enlarges the receptive field by incorporating an appearance-enhanced axis-wise learning block into the encoder and adopting a hybrid-transformer decoder. Experimental results on four datasets demonstrate that our AEMatter significantly outperforms state-of-the-art matting methods (e.g., on the Adobe Composition-1K dataset, 25% and 40% reduction in terms of SAD and MSE, respectively, compared against MatteFormer). The code and model are available at <https://github.com/QLYoo/AEMatter>.

1. Introduction

Natural image matting aims to estimate the alpha matte of the foreground in a given image for composition. This technology has numerous real-world applications, such as image editing [7, 8] and film post-production [15, 49]. Formally, a given image I can be represented as a combination of a foreground image F and background image B as

$$I_i = \alpha_i F_i + (1 - \alpha_i) B_i \quad (1)$$

where α_i is the alpha matte of the foreground image at pixel i . Since the foreground image F , background image B , and alpha matte α are all unknown, the image matting problem is highly ill-defined. To tackle this challenging prob-

*denotes corresponding author.

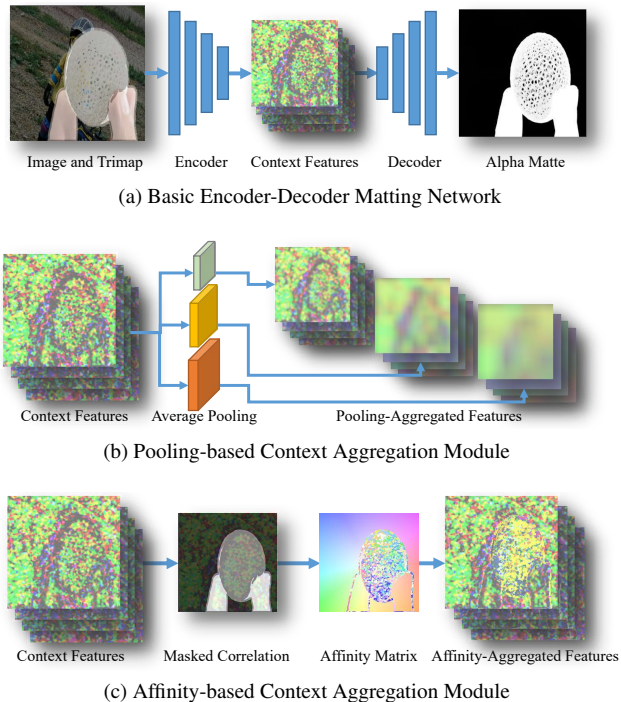


Figure 1: Illustration of a basic matting network and context aggregation modules. (a) The basic matting network uses an encoder to extract context features from inputs, and a decoder to predict alpha mattes. Our AEMatter also follows this scheme. (b) The pooling-based context aggregation module uses average pooling to aggregate contexts from surrounding regions. (c) The affinity-based context aggregation module uses masked correlation to aggregate contexts from globally related regions.

lem, an auxiliary trimap input has been introduced to provide additional information that specifies the known foreground regions, known background regions, and unknown regions in the given image. Existing trimap-based matting methods can be broadly categorized into three categories: sampling-based methods, propagation-based methods, and deep learning-based methods.

Sampling-based methods [2, 39, 9, 46, 14] and

propagation-based methods [16, 22, 23, 18, 6] estimate alpha mattes by sampling foreground and background colors based on location and color similarity or propagating color information in a local region, respectively. However, these traditional methods struggle with scenarios where foreground and background color distributions overlap in local regions. Deep learning-based methods [52, 31] use an encoder to extract context features from the input and then estimate the alpha matte through a decoder, as shown in Figure 1(a). Due to the powerful representation ability of the learned context features, these methods significantly outperform traditional sampling-based and propagation-based methods. Recently, some attempts focus on refining context features to further improve performance in challenging scenarios [4, 25, 13, 53, 30, 34]. These studies usually adopt specifically designed pooling-based or affinity-based context aggregation modules, as illustrated in Figures 1(b) and 1(c). Despite the excellent performance achieved by these matting networks, the effectiveness of the context aggregation modules has not been fully explored.

In this paper, we first conduct extensive experiments and find that the context aggregation modules do not significantly improve the performance, which reveals the limited effectiveness of these modules. Furthermore, we evaluate basic encoder-decoder matting networks with various backbones and find that these networks can learn from large training image patches to aggregate context. We also observe that a matting network with a larger receptive field can achieve better performance. Based on these findings, we propose a simple yet effective matting network without relying on any context aggregation modules, named AEMatter, which enlarges the receptive field by incorporating an appearance-enhanced axis-wise learning block into the encoder and adopting a hybrid-transformer decoder. Extensive experimental results on four datasets, namely Adobe Composition-1K [52], Distinctions-646 [37], Transparent-460 [3], and Semantic Image Matting [43] demonstrate that the proposed AEMatter significantly outperforms state-of-the-art matting methods by a large margin.

To summarize, the contributions of this paper are as follows:

- We present the first empirical analysis of the context aggregation modules in matting networks, and reveal their limited effectiveness. Additionally, we demonstrate that basic encoder-decoder networks can learn from large image patches to effectively aggregate context and achieve high performance.
- We propose a simple yet effective matting network, named AEMatter, which enlarges the receptive field by incorporating an appearance-enhanced axis-wise learning block into the encoder and adopting a hybrid-transformer decoder.

- Extensive experimental results demonstrate that our AEMatter significantly outperforms state-of-the-art methods. Taking the Adobe Composition-1K dataset as an example, AEMatter achieves **25%** and **40%** reduction in terms of SAD and MSE, respectively, compared against MatteFormer.

2. Related Work

Sampling-based methods. Sampling-based methods [2, 39, 46, 14, 17, 41] samples candidate foreground and background colors for pixels in the unknown regions for alpha matte estimation. To improve the robustness, researchers have made a lot of improvements to the sampling strategy. Berman *et al.* [2] propose to estimate the alpha matte with the known pixels sampled around unknown pixels as candidate foreground and background colors. Bayesian Matting [9] models the foreground and background color with a Gaussian distribution, and introduces spatial location information to help improve accuracy. Global Matting [17] proposes to sample the pixels in all known regions to avoid information loss and improve the robustness.

Propagation-based methods. Propagation-based methods [42, 16, 22, 23, 18, 6, 24, 1] use the assumption that the foreground and background colors are smooth in the local regions to estimate the alpha matte. To facilitate inference and improve speed, researchers have constructed many optimized object functions for estimating the alpha matte. Poisson Matting [42] uses the boundary information from the given trimap to solve the Poisson equation, which helps to estimate the alpha matte with rough trimap. Close-form matting [22] introduces a color-line assumption and provides a closed-form solution for alpha matte estimation. He *et al.* [18] use a large kernel of the Laplace matrix to reduce the number of iterations, which speeds up the inference.

Deep learning-based methods. Deep learning-based methods [52, 33, 25, 13, 43, 4, 44, 27, 47, 10, 21] train the networks on image matting datasets to estimate the alpha matte. Early methods [52, 31] typically employ a basic encoder-decoder network and modify the network structure to improve performance. DIM [52] introduced a refinement module to the decoder to improve the performance. IndexNet [31] retains the indices of the downsampled features for upsampling features, which improves the gradient accuracy of the predicted alpha matte. Recent advancements in deep image matting methods have designed pooling-based or affinity-based context aggregation modules to refine context features and adopt other techniques to improve performance. Pooling-based methods [13, 54, 43, 30, 34, 3] use average pooling to aggregate contexts from surrounding regions for context feature refinement. FBAMatting [13] adopts pyramid pooling module (PPM) [56] and introduces the groupnorm [50] and weight standardization [36] tricks to improve the matting performance. SIM [43] adopts

Atrous Spatial Pyramid Pooling (ASPP) [5] and uses semantic segmentation of the image to help to predict alpha mattes. MGMatting [54] adopts ASPP and designs a progressive refinement decoder to estimate fine alpha mattes from coarse segmentation. LFPNet [30] proposes a center-surround pyramid pooling to aggregate long-range contexts to help estimate the alpha matte. MatteFormer [34] proposes a trimap-guided token pooling module and adopts the Swin-Tiny [29] backbone to improve the prediction. TransMatting [3] proposes a global-pooling guided fusion module to improve the prediction for transparent objects. Affinity-based methods [25, 53, 55, 11] use the masked correlation to construct an affinity matrix and enhance the context features with the contexts from globally related regions. GCAMatting [25] adopts the guided context attention module to improve the prediction in the transparent region. HD-Matt [53] proposes a cross-patch feature association module to implement patch-based alpha matte estimation. TIMI-Net [28] proposes a tripartite information module and multi-branches architecture to improve the estimated alpha matte. RMat [11] proposes a low-level feature assembling module and the Segformer [51] backbone as well as strong data augmentation to improve the robustness.

3. Empirical Study

We aim to assess the context aggregation mechanism of matting networks from the perspective of the network architecture. To this end, we conduct diagnostic experiments to analyze the effectiveness of the context aggregation modules. Furthermore, we compare basic encoder-decoder networks with state-of-the-art networks to understand the impact of network design on performance.

3.1. Exploring Context Aggregation Module

To advance the understanding of the context aggregation mechanism in matting networks, we conduct diagnostic experiments on existing matting networks under multi-configuration and analyze the results.

Patch-based Inference. Existing matting networks utilize context aggregation modules to refine context features by aggregating the contexts in large regions, which helps to improve the estimation. In this regard, a large amount of context information contributes to the refinement of context features in the local regions, ultimately improving the overall performance of the matting networks. Existing matting networks process whole images during inference, which preserves all context information. However, when image patches are extracted from these images, the context information is lost, leading to a decline in the performance of the matting methods. In light of this, we evaluate the effectiveness of context aggregation modules in existing matting methods through patch-based inference experiments.

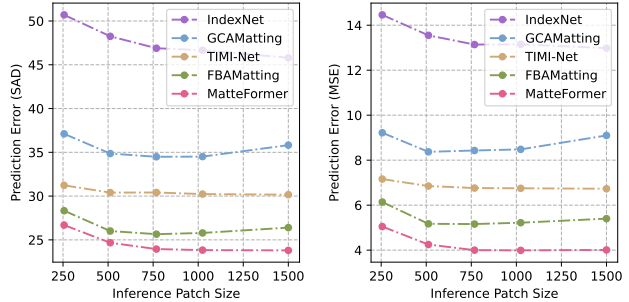


Figure 2: **Inference Patch Size vs Prediction Errors.** As the inference patch size increases, the prediction errors of the compared matting methods [31, 25, 28, 13, 34] first decrease and then remain flat.

We evaluate existing matting methods, including IndexNet [31] without a context aggregation module and GCAMatting [25], TIMI-Net [28], FBAMatting [13], and MatteFormer [34] with a context aggregation module. The evaluation was conducted on image patches of varying sizes, ranging from 256×256 , 512×512 , 768×768 , and 1024×1024 , and on the whole images. The results are summarized in Figure 2, and show a decrease in errors for all methods as the patch size increases until stabilization. Remarkably, the matting networks with context aggregation modules do not result in a significant alteration in the performance trend when compared to IndexNet without such modules, which indicates that these modules have limited effectiveness to utilize the context information during inference and do not significantly improve performance.

Patch-based Training. Context aggregation modules are also designed to aggregate context information to refine the context features for the decoders during the training stage, ultimately improving matting performance. However, existing methods use cropped image patches for training, which leads to limited context features extracted by the encoders. As a result, the matting networks with context aggregation modules only learn to predict alpha mattes with partially refined context features, which may not achieve optimal performance when applied to the whole image. In contrast, the matting networks without context aggregation modules make predictions based solely on the locally extracted context features, which may not be affected by patch-based training. Hence, we hypothesize that a network with a context aggregation module demonstrates improved performance trends when trained on large image patches compared to a network without such modules. To validate this hypothesis, we evaluate existing matting networks with and without context aggregation modules that are trained on image patches of different sizes.

We evaluate IndexNet without a context aggregation

Table 1: Comparison of state-of-the-art matting methods [31, 13, 34] trained on Adobe Composition-1K dataset using image patches of different sizes.

Method	Patch Size	SAD	MSE	Grad	Conn
IndexNet [31]	256	38.52	8.74	18.02	36.43
IndexNet [31]	512	33.64	7.05	14.35	30.21
IndexNet [31]	768	31.12	6.40	12.83	27.63
IndexNet [31]	1024	30.91	6.73	13.72	27.17
FBAMatting [13]	256	43.18	10.41	21.13	42.39
FBAMatting [13]	512	33.36	7.26	15.75	29.84
FBAMatting [13]	768	29.89	5.73	14.05	26.18
FBAMatting [13]	1024	30.76	5.74	15.19	27.03
MatteFormer [34]	256	28.52	5.51	12.00	24.06
MatteFormer [34]	512	23.61	3.78	9.23	18.52
MatteFormer [34]	768	22.78	3.59	8.38	17.50
MatteFormer [34]	1024	23.68	3.62	8.81	18.66

module and FBAMatting and MatteFormer with a context aggregation module. All compared methods are first trained on image patches with sizes of 256×256 , 512×512 , 768×768 , and 1024×1024 , and then evaluated on the validation set. Note that, we do not introduce the auxiliary task of predicting foreground and background when training FBAMatting. The results are summarized in Table 1. We can observe that the performance of all methods exhibits an upward trend followed by stability as the training data size increases. In particular, all compared methods show very little performance improvement when the size of the training data achieves 1024×1024 , and the trends of the networks with and without context aggregation modules are similar. These results contradict our hypothesis that the context aggregation module could enhance network performance by utilizing contexts across large regions. Therefore, the context aggregation modules have little effect on the training of the matting networks, as the networks without these modules also achieve good performance with large training image patches.

3.2. Exploring Basic Matting Network

Based on the above experiments, we hypothesize that basic encoder-decoder networks can learn from large training image patches to aggregate context for alpha matte estimation. To validate the hypothesis, we construct several basic encoder-decoder matting networks using the backbones employed by existing matting methods [31, 25, 10, 13, 34] and compare them with current state-of-the-art matting methods. Specifically, we adopt MobileNet [40], ResNet-34 [20], ResNet-50 [20], and Swin-Tiny [29] to construct basic matting networks without any context aggregation modules. Note that, we simply adopt IndexNet as the MobileNet based basic matting network. Then, we follow the training pipeline of GCAMatting to train the basic matting

Table 2: Comparison of the basic matting networks with state-of-the-art matting methods [31, 25, 10, 28, 13, 43, 48, 34, 3] on Adobe Composition-1K. * denotes the backbone adopts the dilated convolution trick.

Method	Backbone	SAD	MSE	Grad	Conn
IndexNet [31]	MobileNet	45.80	13.00	25.90	43.70
BasicNet (Ours)	MobileNet	30.91	6.73	13.72	27.17
GCAMatting [25]	ResNet-34	35.28	9.00	16.90	32.50
A2UNet [10]	ResNet-34	32.10	7.80	16.33	29.00
TIMI-Net [28]	ResNet-34	29.08	6.00	11.50	25.36
BasicNet (Ours)	ResNet-34	28.08	5.06	11.39	24.32
SIM [43]	ResNet-50*	28.00	5.80	10.8	24.80
FBAMatting [13]	ResNet-50*	26.40	5.40	10.6	21.50
LSAMatting [48]	ResNet-50	25.90	5.40	9.25	21.50
BasicNet (Ours)	ResNet-50	23.82	4.27	8.08	19.02
Transmatting [3]	Swin-Tiny	26.83	5.22	10.62	22.14
MatteFormer [34]	Swin-Tiny	23.80	4.03	8.68	18.90
BasicNet (Ours)	Swin-Tiny	19.72	2.97	6.27	14.43

networks on image patches with the size of 1024×1024 . Finally, we compare these basic networks with state-of-the-art networks including, IndexNet, GCAMatting, FBAMatting, A2UNet [10], TIMI-Net, FBAMatting, LSAMatting [48], and MatteFormer. As the results summarized in Table 2 show, our basic networks (referred to as BasicNet in the table) significantly outperform the state-of-the-art networks that adopt the same backbones. Furthermore, the Swin-Tiny based network outperforms the MobileNet, ResNet-34, and ResNet-50 based networks and achieves a new state-of-the-art performance, which indicates that a network that has a larger receptive field can better learn context aggregation to achieve higher performance. In the appendix, we provide more detailed analysis of the effect of training patch size and receptive field on the performance, and compare the robustness of the basic networks and state-of-the-art networks to coarse trimaps.

3.3. Experimental Findings

Based on the experimental results presented above, we have three main findings: (1). Our experiments reveal that the context aggregation module has limited impacts on both the inference and training phases of matting networks, which indicates that these modules are not necessary. (2). We demonstrate that basic encoder-decoder networks without aggregation modules can outperform state-of-the-art matting methods, which shows the ability of these basic networks to learn to aggregate context from large training image patches. (3). We find that the matting networks built on the Swin-Tiny backbone exhibit high performance, which highlights the importance of a network with a large receptive field for image matting. These findings motivate us to design a simple yet effective network.

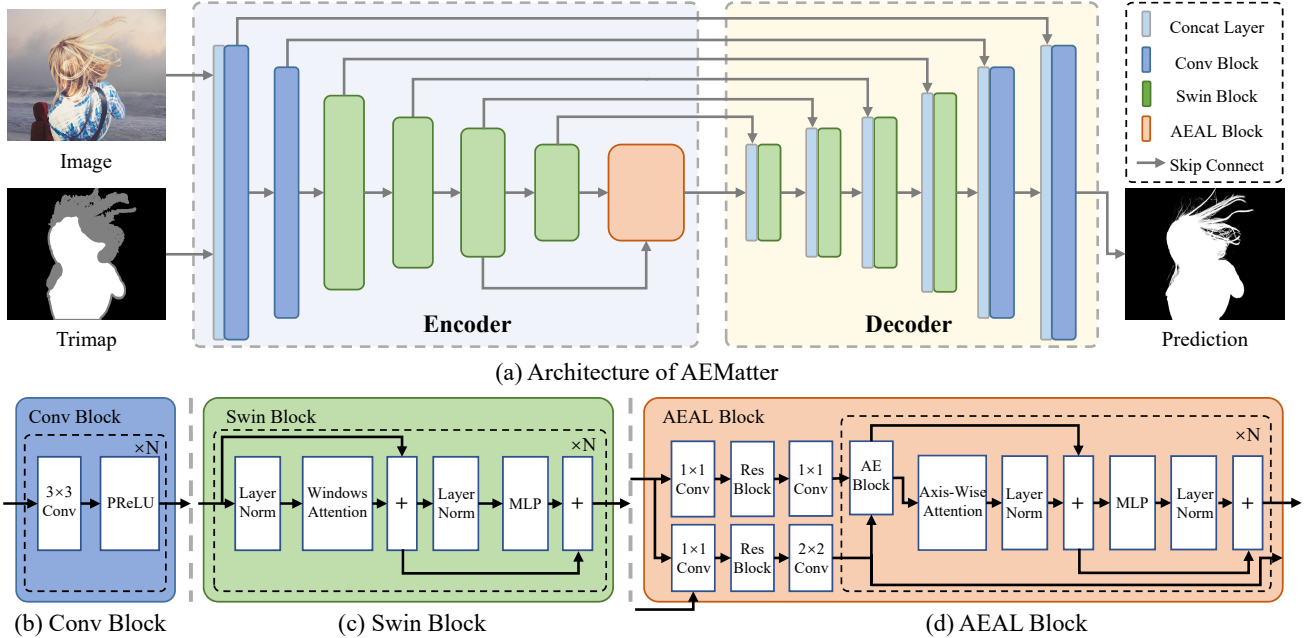


Figure 3: Overview of AEMatter. AEMatter adopts a basic encoder-decoder architecture. The encoder first adopts a stem-enhanced Swin-Tiny backbone with an appearance-enhanced axis-wise learning (AEAL) block to extract context features. The decoder then adopts a hybrid-Transformer structure to refine the context features and estimate the alpha matte.

4. Proposed Method

As illustrated in Figure 3(a), our AEMatter adopts a basic encoder-decoder architecture. The encoder adopts a stem-enhanced backbone with an appearance-enhanced axis-wise learning (AEAL) block to extract context features. The decoder adopts a hybrid-Transformer to refine the context features and estimate the alpha matte.

4.1. Encoder

To extract low-level features and context features from the inputs and enlarge the receptive field, we adopt a stem-enhanced backbone with an appearance-enhanced axis-wise learning (AEAL) block to construct the encoder.

4.1.1 Stem-Enhanced Backbone

Although the Swin-Tiny [29] based matting network performs best in the above experiments, Swin-Tiny is primarily designed for high-level semantic tasks and ignores extracting low-level features, which limits its effectiveness in image matting. Prior studies [34, 11] address this issue by incorporating additional shortcut modules to extract low-level features, but their backbones cannot utilize the shortcut features, resulting in subpar performance. In contrast, we replace the patch-embedding stem with convolution blocks to extract rich low-level features. The structure of the convolution block is illustrated in Figure 3(b). To preserve the im-

age details, we omit the normalization layers in the stem as they cause internal covariate shift, which hurts the matting performance. To overcome the gradient vanishing issue resulting from the absence of normalization, we incorporate PReLU [19] as the activation function, which introduces learnable negative slopes to facilitate network training. Afterward, we use the Swin blocks of Swin-Tiny to extract high-level context features.

4.1.2 Appearance-Enhanced Axis-Wise Learning

The Swin-Tiny based backbone adopts the hierarchical structure that is effective in capturing and integrating context features within nearby spatial regions. However, its limited receptive field limits the performance of the matting network. While one possible solution to this issue is to employ more downsampling layers and Swin blocks to extract context features across larger regions, such an approach can hinder the training and increase the risk of overfitting. To address this issue, we incorporate an appearance-enhanced axis-wise learning (AEAL) block after the Swin-Tiny backbone, which leverages an appearance-enhanced (AE) block to facilitate training and axis-wise attention to further enlarge the receptive fields.

The structure of AEAL block is illustrated in Figure 3(d). To mitigate high computational overheads incurred by the high-dimension context features from the backbone, we use residual blocks and 1×1 convolutions to produce the com-

pressed the context features F_c from the fourth-stage features F_4 of the backbone. Additionally, we use F_4 to guide the extraction of appearance features from third-stage features F_3 of the backbone with convolution and residual blocks, generating the context-guided appearance features F_a . Subsequently, we employ three cascaded learning modules to process F_c and F_a . To facilitate network training, we first introduce an AE block to generate the appearance-enhanced context features F_{ac} with F_c and F_a as

$$F_{ac} = F_c + \text{Conv}(\text{Res}(\text{Conv}(\text{Cat}(F_c, F_a)))) \quad (2)$$

where $\text{Cat}(\cdot, \cdot)$, $\text{Conv}(\cdot)$, and $\text{Res}(\cdot)$ denote the concatenation, 1×1 convolution, residual block, respectively. To capture context features over large regions, we propose axis-wise attention, which involves dividing F_{ac} into axis-wise rectangular regions and applying multi-head self-attention. Specifically, we first zero-pad F_{ac} to a size that is an integer multiple of width W , then split the padded feature F_{acp} into two features, F_{acpx} and F_{acpy} , along the channel dimension. These two features are then further divided into two sets of axis-wise features $F_{cx}^1, F_{cx}^2, \dots, F_{cx}^{n_x}$ and $F_{cy}^1, F_{cy}^2, \dots, F_{cy}^{n_y}$, respectively. Next, we apply multi-head self-attention to process the features within each set, which are re-assembled to form the refined context feature F_{rc} . Finally, we adopt the MLP network as the FPN for feature transformation, following the vanilla Transformer [45].

4.2. Decoder

To further enlarge the receptive field of AEMatter and improve the alpha matte estimation, we adopt a hybrid-Transformer decoder that employs Swin blocks which have a large receptive field to refine the context features from the encoder and convolution blocks for predicting. Specifically, we first concatenate the refined context feature F_{rc} with the fourth-stage features F_4 from the encoder, and apply Swin blocks to generate the initial decoder feature F_d . We then upsample F_d and concatenate it with the features of the corresponding scale of the encoder, and apply another Swin blocks for feature refinement. This process is repeated three times to obtain the refined decoder features F_{rd} . To fuse the image details for alpha matte estimation, we upsample F_{rd} and concatenate it with the low-level features extracted by the stem of the encoder, and process it using convolution blocks that omit the normalization layers to avoid internal covariate shift. We perform this process twice and then use a 3×3 convolution to predict the alpha matte α . Finally, we clip the predicted alpha matte α to the range of 0 to 1 using the clamp operation.

4.3. Loss Functions

To train the proposed AEMatter, we follow existing methods [52, 13] to construct the network loss \mathcal{L}_α as

$$\mathcal{L}_\alpha = \mathcal{L}_{l1} + \mathcal{L}_{cb} + \mathcal{L}_{lap} \quad (3)$$

where \mathcal{L}_{l1} , \mathcal{L}_{cb} , and \mathcal{L}_{lap} are the L1 loss, Charbonnier L1 loss, and Laplacian loss, which are defined as

$$\mathcal{L}_{l1} = |\alpha - \alpha^{gt}| \quad (4)$$

$$\mathcal{L}_{cb} = \frac{1}{|\mathcal{T}^U|} \sum_{i \in \mathcal{T}^U} \sqrt{(\alpha_i - \alpha_i^{gt})^2 + \epsilon^2} \quad (5)$$

$$\mathcal{L}_{lap} = \sum_j 2^j |L_j(\alpha) - L_j(\alpha^{gt})| \quad (6)$$

where α and α^{gt} are the predicted alpha matte and ground truth alpha matte of the input image I , respectively. \mathcal{T}^U denotes a set of indices of the unknown pixels in the trimap. ϵ is the Charbonnier penalty coefficient. $L_j(\alpha)$ and $L_j(\alpha^{gt})$ are the j -th level of the Laplacian pyramid representations of α and α^{gt} , respectively.

5. Experiments

In this section, we present a comprehensive evaluation of the proposed AEMatter. First, we provide the implementation details of AEMatter. Then, we compare the performance and generalization ability of our AEMatter with state-of-the-art matting methods on four popular datasets, namely Adobe Composition-1K [52], Distinctions-646 [37], Transparent-460 [3], and Semantic Image Matting [43]. Finally, we conduct ablation studies to verify the effectiveness of the network components of AEMatter. Note that the appendix includes more qualitative results and model complexity analysis.

5.1. Implementation Details

The proposed AEMatter is implemented using the PyTorch [35] framework. Axis-wise attention with a width of $W = 5$ is used in the implementation. The coefficients in the loss functions are set as $\epsilon = 10^{-6}$, and $j = 4$. The network weights are initialized using the Kaiming initializer [19]. To avoid overfitting, the backbone weights are initialized with the weights pre-trained on the ImageNet [12] dataset. The training is conducted on the Adobe Composition-1K dataset [52], using an NVIDIA RTX 3090 GPU with a batch size of 2 for 100 epochs. The RAdam optimizer [26] is employed to optimize the network weights with weight decay of 10^{-6} and betas of (0.5, 0.999). The initial learning rate is set to 2.5×10^{-5} and decays to zero using a cosine annealing scheduler. Data augmentation techniques, including random affine transformation, random saturation transformation, random grayscale transformation, random gamma transformation, random contrast transformation, and random composition are applied to the training data. The trimap is generated from the alpha matte ground truth using erosion and dilation with kernel sizes ranging from 1 to 30 pixels. To facilitate network training, the image and trimap are randomly cropped into patches of size 1024×1024 and fed to the network.

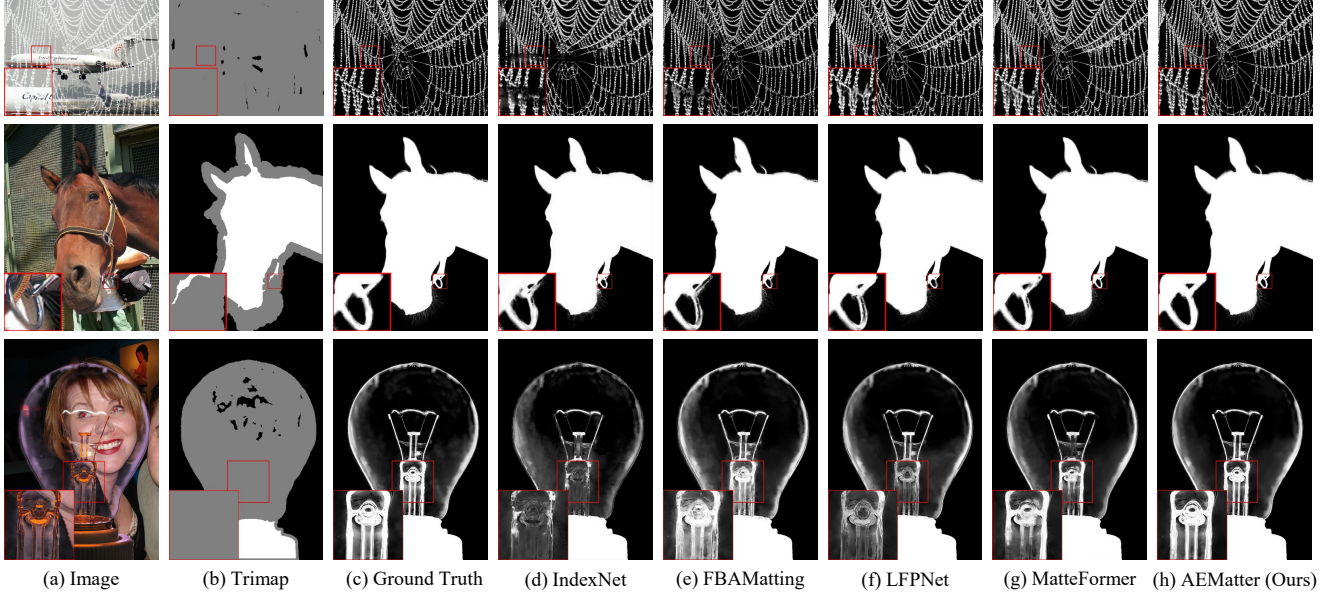


Figure 4: Qualitative comparison of the alpha matte results on the Adobe Composition-1K dataset.

Table 3: Quantitative results on Adobe Composition-1K.

Method	SAD	MSE	Grad	Conn
DIM [52]	50.40	17.00	36.70	55.30
IndexNet [31]	45.80	13.00	25.90	43.70
GCAMatting [25]	35.28	9.00	16.90	32.50
TIMI-Net [28]	29.08	6.00	11.50	25.36
SIM [43]	27.70	5.60	10.70	24.40
FBAMatting [13]	26.40	5.40	10.60	21.50
LSAMatting [48]	25.90	5.40	9.25	21.50
TransMatting [3]	24.96	4.58	9.72	20.16
LFPNet [30]	23.60	4.10	8.40	18.50
MatteFormer [34]	23.80	4.03	8.68	18.90
RMat [11]	22.87	3.90	7.74	17.84
AEMatter (Ours)	17.79	2.39	4.81	12.64

5.2. Results on Adobe Composition-1K

We compare AEMatter with state-of-the-art matting methods, including DIM [52], IndexNet [31], GCAMatting [25], FBAMatting [13], SIM [43], TIMI-Net [28], LFPNet [30], LSAMatting [48], MatteFormer [34], and RMat [11] on the Adobe Composition-1K dataset. Table 3 and Figure 4 summarize the quantitative and qualitative results of all compared matting methods. Our AEMatter significantly outperforms state-of-the-art methods with its exceptional performance in terms of SAD, MSE, Grad, and Conn metrics. Moreover, AEMatter produces visually appealing alpha mattes, especially in regions where the foreground and background colors are very similar.

Table 4: Generalization results on the Distinction-646. All methods are trained on Adobe Composition-1K.

Method	SAD	MSE	Grad	Conn
DIM [52]	63.88	25.77	53.23	66.31
IndexNet [31]	44.93	9.23	41.30	44.86
TIMI-Net [28]	42.61	7.75	45.05	42.40
GCAMatting [25]	36.37	8.19	32.34	36.00
FBAMatting [13]	32.28	5.66	25.52	32.39
LFPNet [30]	22.36	3.41	14.92	20.50
Matteformer [34]	23.60	3.12	13.56	21.56
AEMatter (Ours)	18.97	2.17	10.05	17.02

5.3. Generalization on Various Datasets

We evaluate the generalization ability of DIM, IndexNet, GCAMatting, FBAMatting, LFPNet, MatteFormer, and our proposed AEMatter on the Distinctions-646, Transparent-460, and Semantic Image Matting datasets. All compared methods are pre-trained on Adobe Composition-1K and the trimaps for Distinctions-646 and Semantic Image Matting are generated using morphological operations. We present the quantitative results in Tables 4, 5, and 6. Additionally, we provide the qualitative results in the appendix. The results clearly demonstrate that AEMatter outperforms state-of-the-art methods, which indicates its exceptional generalization ability.

5.4. Results on Real-world Images

To comprehensively assess the performance of AEMatter in real-world scenarios, we conduct a comparative study

Table 5: Generalization results on Transparent-460. All methods are trained on Adobe Composition-1K.

Method	SAD	MSE	Grad	Conn
DIM [52]	356.20	49.68	146.46	296.31
IndexNet [31]	434.14	74.73	124.98	368.48
TIMI-Net [28]	328.08	44.20	142.11	289.79
MGMatting [54]	344.65	57.25	74.54	282.79
TransMatting [3]	192.36	20.96	41.80	158.37
AEMatter (Ours)	125.73	7.13	35.61	115.13

Table 6: Generalization results on Semantic Image Matting. All methods are trained on Adobe Composition-1K.

Method	SAD	MSE	Grad	Conn
DIM [52]	95.96	54.25	29.84	100.65
IndexNet [31]	66.89	25.75	22.07	67.61
GCAMatting [25]	51.84	19.46	24.16	51.98
FBAMatting [13]	26.87	5.61	9.17	22.87
TIMI-Net [28]	54.08	16.59	18.91	53.79
LFPNet [30]	23.05	4.28	23.30	18.19
Matteformer [34]	23.90	4.73	7.72	19.01
AEMatter (Ours)	19.80	2.89	4.72	14.89

with state-of-the-art MatteFormer on real-world images. We first collect high-resolution real-world images from the internet and manually annotate them with trimaps. Then, we qualitatively evaluate AEMatter and MatteFormer on these data. The results, as shown in Figure 5, demonstrate that AEMatter achieves significantly higher prediction accuracy than MatteFormer, highlighting its immense potential for practical applications, such as image editing.

5.5. Ablation Study

Hybrid-Transformer Decoder. We introduce a hybrid-transformer decoder to enlarge the receptive field of the decoder. To evaluate the effectiveness of this design, we evaluate AEMatter with convolution, residual block, and hybrid-transformer decoders and summarize the results in Table 7. Experimental results demonstrate that our hybrid-transformer decoder outperforms the other two designs.

Appearance-Enhanced Axis-Wise Learning. We introduce an AEAL block to enlarge the receptive field of the encoder, which adopts AE blocks to enhance the appearance information of context features and axis-wise attention to learn large-scale contexts. To evaluate the effectiveness of these designs, we evaluate AEMatter, AEMatter without AE blocks, AEMatter with the vanilla self-attention [45] or the window attention [29] on Adobe Composition-1K, as summarized in Table 7. Experimental results demonstrate that AEMatter with axis-wise attention outperforms

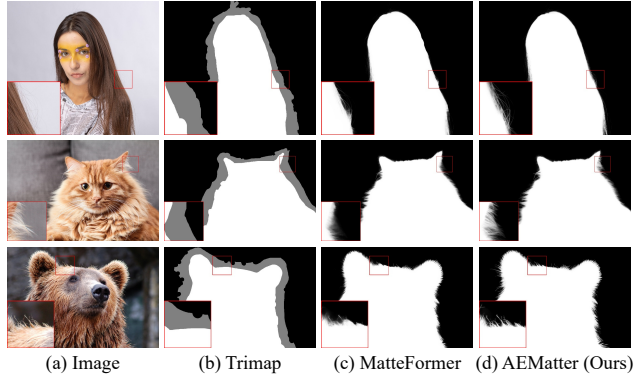


Figure 5: Qualitative comparison of the alpha matte results on real-world images.

Table 7: Ablation study on the decoder architecture and additional learning blocks. Decoder denotes the decoder adopted, AL denotes the additional learning block adopted, and AE denotes whether the appearance-enhanced block is used. The additional learning blocks considered are Vanilla, Window, and Axis, representing vanilla self-attention, window attention, and our axis-wise attention, respectively.

Decoder	AL	AE	SAD	MSE	Grad	Conn
Convolution	-	×	19.57	2.76	5.84	14.36
Residual	-	×	19.23	2.82	5.73	14.09
Hybrid-Trans	-	×	18.91	2.66	5.13	13.87
Hybrid-Trans	Vanilla	×	19.07	2.65	5.86	13.92
Hybrid-Trans	Window	×	18.30	2.61	5.56	13.11
Hybrid-Trans	Axis	×	18.09	2.51	5.04	13.05
Hybrid-Trans	Axis	✓	17.79	2.39	4.81	12.64

AEMatter with the vanilla self-attention and window attention, and that the AE block further improves performance, highlighting the effectiveness of the proposed AEAL block.

6. Conclusion

In this paper, we present a comprehensive study on context aggregation modules of matting networks. We conduct extensive experiments and find that the context aggregation modules do not significantly improve the performance, which reveals the limited effectiveness of these modules. We also demonstrate that when learned on large image patches, basic encoder-decoder networks with a larger receptive field can effectively aggregate context to achieve better performance. Based on these findings, we propose a new matting network, named AEMatter, which utilizes an appearance-enhanced encoder and a hybrid-transformer decoder to improve the matting performance by enlarging the receptive field. Extensive experimental results on four datasets demonstrate our AEMatter significantly outperforms state-of-the-art matting methods.

Appendix

The appendix complements the main text by presenting additional analysis and qualitative results. We begin by providing more analysis on basic encoder-decoder matting networks in Section A. Then, we provide the model complexity analysis of the proposed AEMatter in Section B. Finally, we provide more qualitative results of AEMatter and the compared methods in Section C.

A. Analysis on Basic Matting Networks

In this section, we present a comprehensive analysis of the basic encoder-decoder matting networks. First, we investigate the impact of varying training image patch sizes on the performance of the basic matting networks. Second, we evaluate the effect of varying receptive field sizes on the performance of the basic matting networks. Third, we compare the robustness of the basic matting networks with state-of-the-art matting networks to coarse trimaps.

A.1. Analysis on Training Image Patch Sizes

In the main text, we explore the impact of varying the training image patch sizes on the performance of existing matting networks. We hypothesize that using larger image patches during training helps the basic network to learn better context aggregation and thus achieve higher performance without relying on context aggregation modules. To validate this hypothesis, we train the Resnet-34 [20] based and Swin-Tiny [29] based basic matting networks on image patches of different sizes, including 256×256 , 512×512 , 768×768 , and 1024×1024 , and evaluate them. The results, summarized in Table 1, show that the performance of the network improves with larger training image patches, which supports our hypothesis. To further investigate the impact of the sizes of training image patches on network performance, we follow Luo et al. [32] to visualize the effective receptive field of the ResNet-34 based networks that are trained on image patches of different sizes using gradient feedback in Figure 1. The visualization also confirms that the networks that are trained on larger image patches learn better context aggregation.

A.2. Analysis on Receptive Field

In the main text, we evaluate multiple basic encoder-decoder matting networks and observe that the networks that have larger receptive fields, such as Swin-Tiny [29] or ResNet-50 [20] based networks, demonstrate better performance. This observation leads us to hypothesize that the performance of a network is positively correlated with its receptive field size. To verify this hypothesis, we compare the performance of basic matting networks with different kernel sizes. Specifically, we build basic matting networks with ResNet-34 [20] and ResNet-50 backbones. Then, we

Table 1: Diagnostic experiment on the size of training image patches.

Backbone	Patch Size	SAD	MSE	Grad	Conn
Resnet-34	256	41.74	12.51	22.51	40.14
Resnet-34	512	33.16	7.08	15.27	29.80
Resnet-34	768	27.70	5.41	11.23	23.89
Resnet-34	1024	28.08	5.06	11.39	24.32
Swin-Tiny	256	27.99	5.30	11.23	23.96
Swin-Tiny	512	22.42	3.72	7.46	17.54
Swin-Tiny	768	20.37	2.96	6.55	16.89
Swin-Tiny	1024	19.72	2.97	6.27	14.43

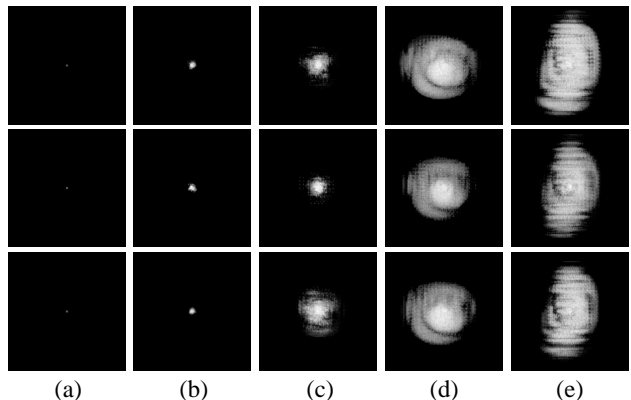


Figure 1: Visualization of the receptive field of basic matting networks trained on image patches of different sizes. (a) Untrained network. (b) Network trained on 256×256 image patches. (c) Network trained on 512×512 image patches. (d) Network trained on 768×768 image patches. (e) Network trained on 1024×1024 image patches.

replace part of 3×3 convolution kernels in these networks with 1×1 convolution kernels and 5×5 convolution kernels to control the receptive field size. We evaluate the performance of the modified networks and summarize the results in Table 2. The results show that the matting network with larger convolution kernels achieves better performance, which provides empirical evidence that supports our hypothesis that networks with larger receptive fields have better performance.

A.3. Robustness to Coarse Trimap

Recent matting research [54, 11] highlights the robustness of matting networks to coarse trimaps. To evaluate whether basic matting networks can handle such trimaps, we compare the performance of the basic encoder-decoder matting networks and existing matting networks on a modified Adobe Composition-1K dataset that has trimaps of varying dilation distances. We compare basic matting networks based on ResNet-34, ResNet-50, and Swin-Tiny

Table 2: Diagnostic experiment on the kernel size.

Backbone	Kernel Size	SAD	MSE	Grad	Conn
Resnet-34	1 × 1	31.28	6.14	13.41	28.05
Resnet-34	3 × 3	28.08	5.06	11.39	24.32
Resnet-34	5 × 5	26.72	4.74	10.08	22.75
Resnet-50	1 × 1	28.70	5.79	10.96	24.98
Resnet-50	3 × 3	23.82	4.27	8.08	19.02
Resnet-50	5 × 5	23.34	3.92	7.42	18.89

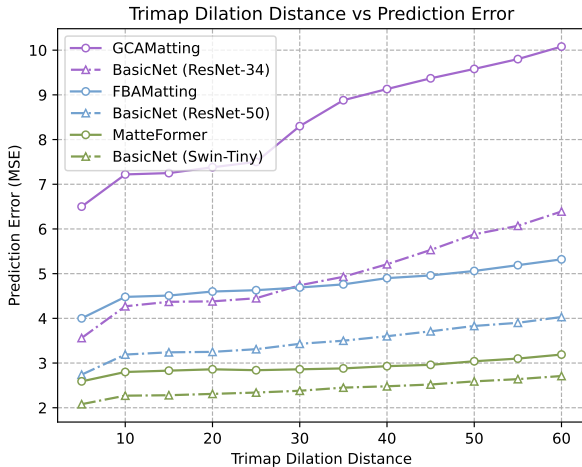


Figure 2: **Trimap Dilation Distance vs Prediction Error.** Note that, the networks with the same backbone are represented by lines with the same color. As the trimap dilation distance increases, the prediction errors (MSE) of all compared matting methods increase.

backbones with state-of-the-art matting methods such as GCAMatting, FBAMatting, and MatterFormer. In Figure 2, we present the results of our comparison study, where we refer to the basic networks as BasicNet. The performance of all matting networks deteriorates as the dilation distance increase. Notably, the state-of-the-art methods with the context aggregation modules do not outperform the basic encoder-decoder network, indicating that the basic matting networks are capable of handling coarse trimaps.

B. Model Complexity

In this section, we analyze the computational complexity and parameter amounts of different image matting methods. We measure the number of multiply-accumulates (MACs) required by each method to infer a 1024×1024 image, as well as the number of trainable parameters in the model. The results, summarized in Table 3, demonstrate that AEMatter has similar computational complexity and parameter amounts to other existing matting methods.

Table 3: Comparison of the computational complexity and parameter amounts of image matting methods.

Method	MACs (G)	Params (M)
DIM [52]	727.4	130.5
IndexNet [31]	116.6	8.2
GCAMatting [25]	257.3	24.1
FBAMatting [13]	686.0	34.8
SIM [43]	1001.9	44.5
TIMI-Net [28]	351.3	35.0
LFPNet [30]	1539.4	112.2
MatteFormer [34]	233.3	44.9
AEMatter (Ours)	295.4	52.0

C. Results on Image Matting Datasets

In this section, we present additional qualitative results on matting datasets. We summarize the comparison results on Distinction-646 [38], Transparent-460 [3], and Semantic Image Matting [43] in Figures 3, 4, and 5, respectively. These figures demonstrate that AEMatter achieves better performance than existing matting methods in predicting alpha mattes for object edges and transparent objects. In addition, we randomly select the predicted alpha mattes of AEMatter on four matting datasets [52, 38, 3, 43] and present them in Figures 6, 7, 8, and 9.

References

- [1] Yagiz Aksoy, Tunc Ozan Aydin, and Marc Pollefeys. Designing Effective Inter-Pixel Information Flow for Natural Image Matting. In *CVPR*, 2017. 2
- [2] Arie Berman, Arpag Dadourian, and Paul Vlahos. Method for removing from an image the background surrounding a selected object, 1998. 1, 2
- [3] Huanqia Cai, Fanglei Xue, Lele Xu, and Lili Guo. TransMatting: Enhancing Transparent Objects Matting with Transformers. In *ECCV*, 2022. 2, 3, 4, 6, 7, 8, 10
- [4] Shaofan Cai, Xiaoshuai Zhang, Haoqiang Fan, Haibin Huang, Jiangyu Liu, Jiaming Liu, Jiaying Liu, Jue Wang, and Jian Sun. Disentangled Image Matting. In *ICCV*, 2019. 2
- [5] Liang-Chieh Chen, George Papandreou, Iasonas Kokkinos, Kevin Murphy, and Alan L. Yuille. DeepLab: Semantic Image Segmentation with Deep Convolutional Nets, Atrous Convolution, and Fully Connected CRFs. *TPAMI*, 40(4):834–848, 2018. 3
- [6] Qifeng Chen, Dingzeyu Li, and Chi-Keung Tang. KNN Matting. *TPAMI*, 35(9):2175–2188, 2013. 2
- [7] Tao Chen, Ming Ming Cheng, Ping Tan, Ariel Shamir, and Shi Min Hu. Sketch2Photo: Internet Image Montage. In *SIGGRAPH ASIA*, 2009. 1

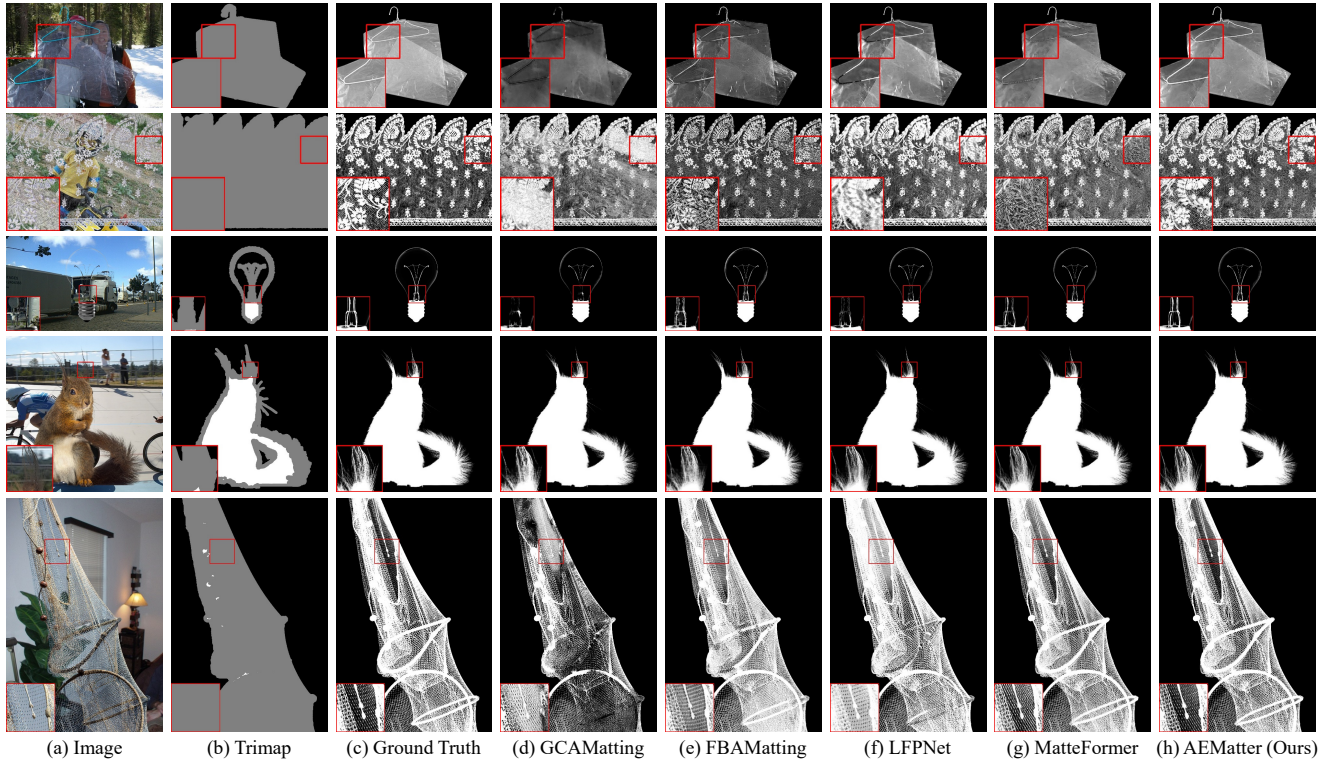


Figure 3: Qualitative comparison of the alpha matte results on the Distinction-646 dataset.

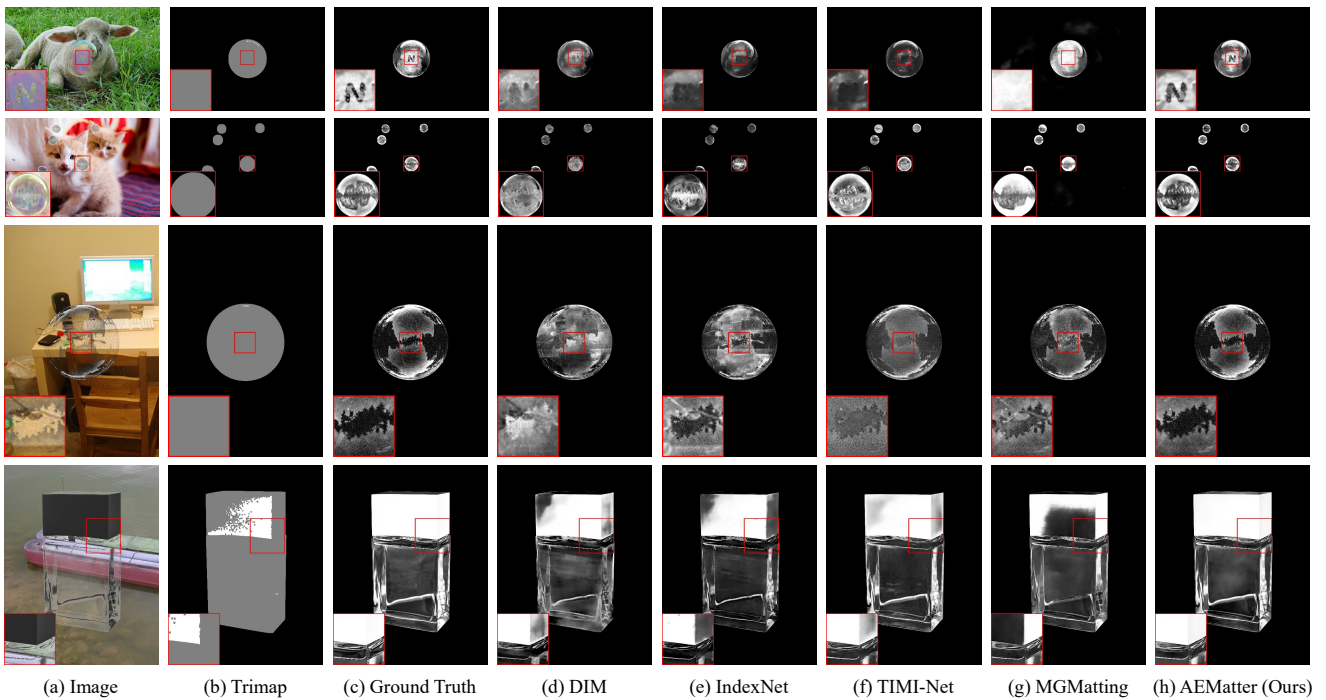


Figure 4: Qualitative comparison of the alpha matte results on the Transparent-460 dataset.

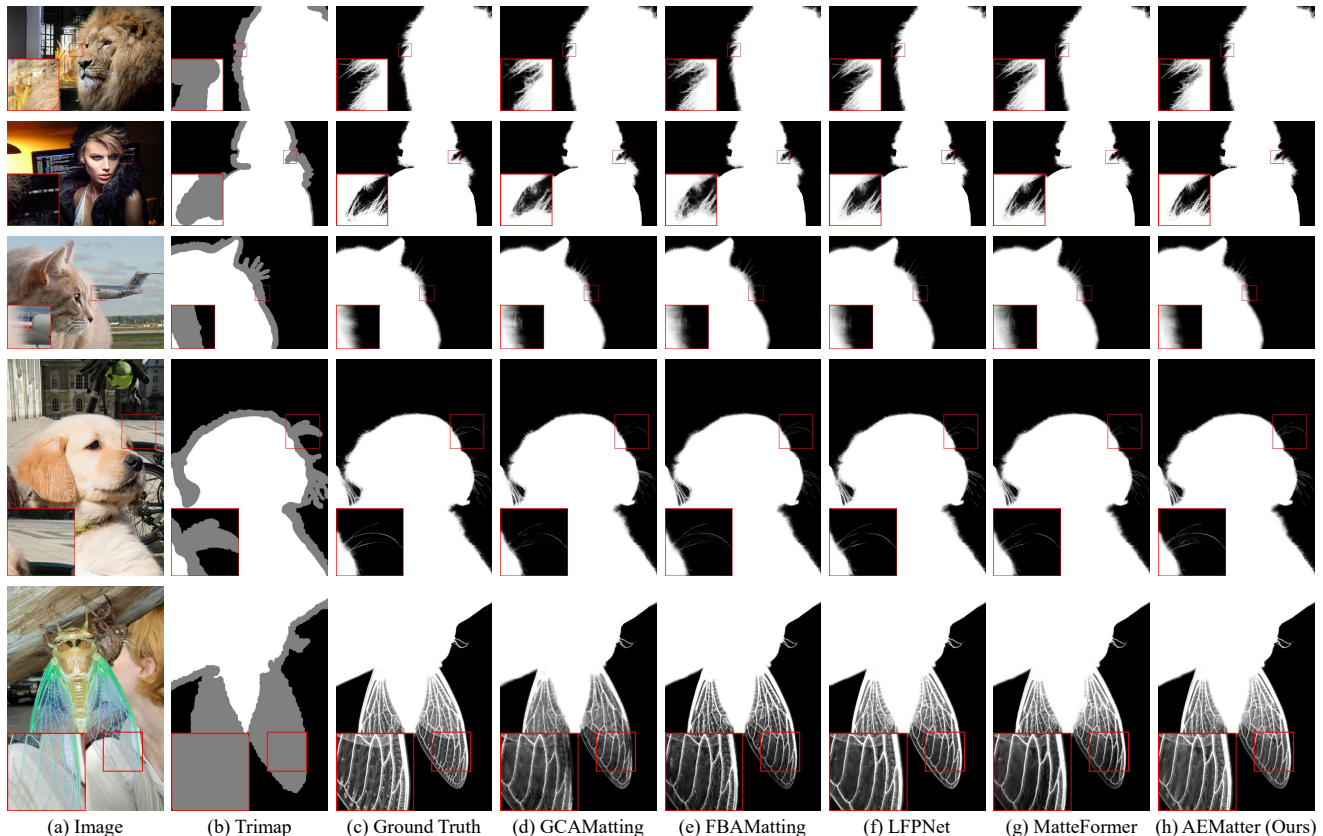


Figure 5: Qualitative comparison of the alpha matte results on the Semantic Image Matting dataset.

- [8] Yibo Chen, Jingwei Guan, and Wai Kuen Cham. Robust Multi-Focus Image Fusion Using Edge Model and Multi-Matting. *TIP*, 27:1526 – 1541, 2018. 1
- [9] Yung-Yu Chuang, B. Curless, D.H. Salesin, and R. Szeliski. A Bayesian Approach to Digital Matting. In *CVPR*, 2001. 1, 2
- [10] Yutong Dai, Hao Lu, and Chunhua Shen. Learning Affinity-Aware Upsampling for Deep Image Matting. In *cvpr*, 2021. 2, 4
- [11] Yutong Dai, Brian Price, He Zhang, and Chunhua Shen. Boosting Robustness of Image Matting with Context Assembling and Strong Data Augmentation. In *CVPR*, 2022. 3, 5, 7, 9
- [12] Jia Deng, Wei Dong, Richard Socher, Li-Jia Li, Kai Li, and Li Fei-Fei. ImageNet: A large-scale hierarchical image database. In *CVPR*, 2009. 6
- [13] Marco Forte and François Pitié. F, B, Alpha Matting. *arXiv preprint arXiv:2003.07711*, 2020. 2, 3, 4, 6, 7, 8, 10
- [14] Eduardo Simoes Lopes Gastal and Manuel M. Oliveira. Shared Sampling for Real-Time Alpha Matting. *Computer Graphics Forum*, 29(2):575–584, 2010. 1, 2
- [15] Minglun Gong, Yiming Qian, and Li Cheng. Integrated Foreground Segmentation and Boundary Matting for Live Videos. *TIP*, 24(4):1356–1370, 2015. 1
- [16] Leo Grady and Rüdiger Westermann. Random Walks for Interactive Alpha-Matting. In *VIIIP*, 2005. 2
- [17] Kaiming He, Christoph Rhemann, Carsten Rother, Xiaoou Tang, and Jian Sun. A Global Sampling Method for Alpha Matting. In *CVPR*, 2011. 2
- [18] Kaiming He, Jian Sun, and Xiaoou Tang. Fast Matting Using Large Kernel Matting Laplacian Matrices. In *CVPR*, 2010. 2
- [19] Kaiming He, Xiangyu Zhang, Shaoqing Ren, and Jian Sun. Delving Deep into Rectifiers: Surpassing Human-Level Performance on ImageNet Classification. In *ICCV*, 2015. 5, 6
- [20] Kaiming He, Xiangyu Zhang, Shaoqing Ren, and Jian Sun. Deep Residual Learning for Image Recognition. In *CVPR*, 2016. 4, 9
- [21] Qiqi Hou and Feng Liu. Context-Aware Image Matting for Simultaneous Foreground and Alpha Estimation. In *ICCV*, 2020. 2
- [22] A. Levin, D. Lischinski, and Y. Weiss. A Closed-Form Solution to Natural Image Matting. *TPAMI*, 30(2):228–242, 2008. 2
- [23] Anat Levin, Alex Rav-Acha, and Dani Lischinski. Spectral Matting. *TPAMI*, 30(10):1699–1712, 2008. 2

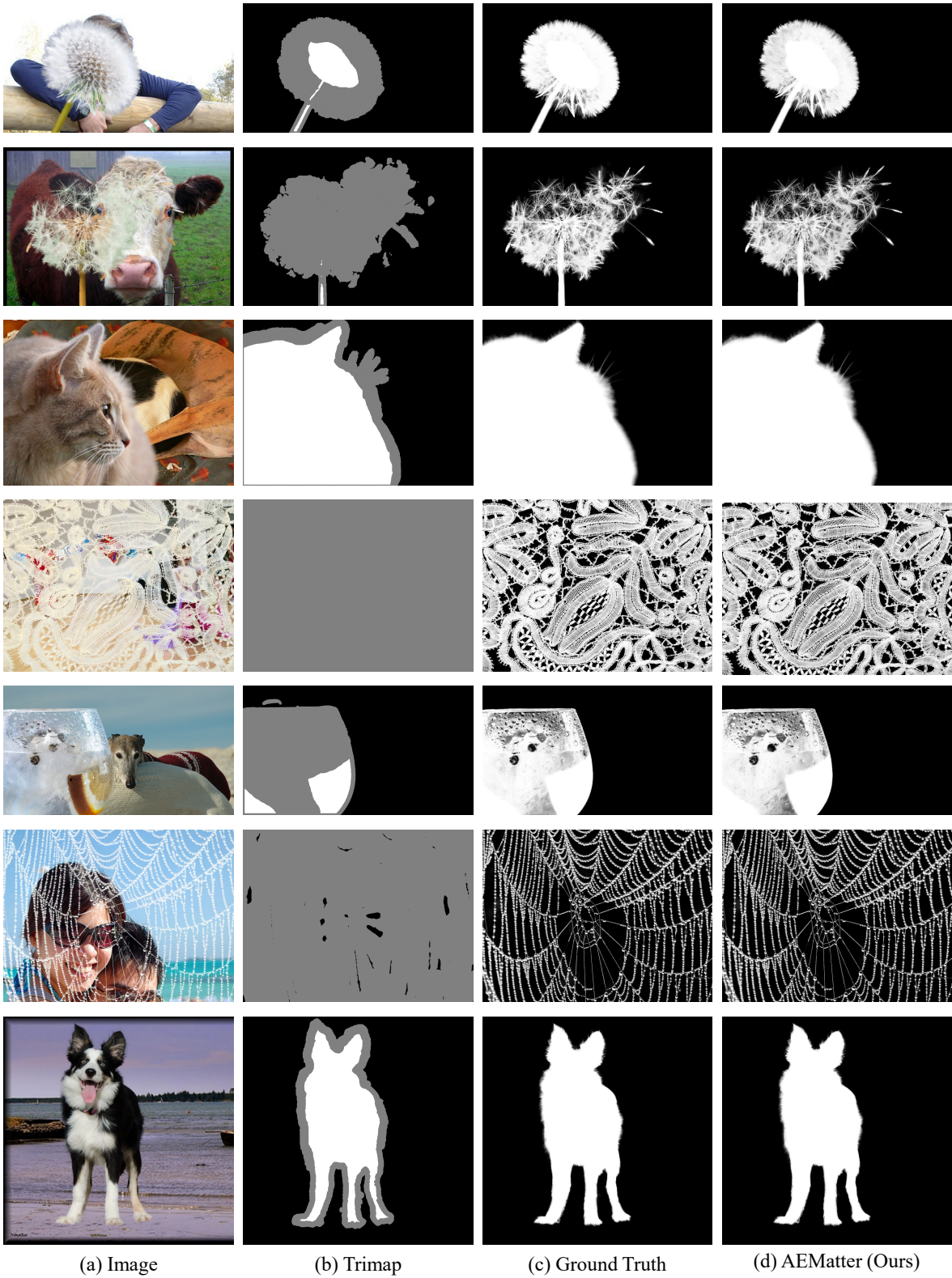
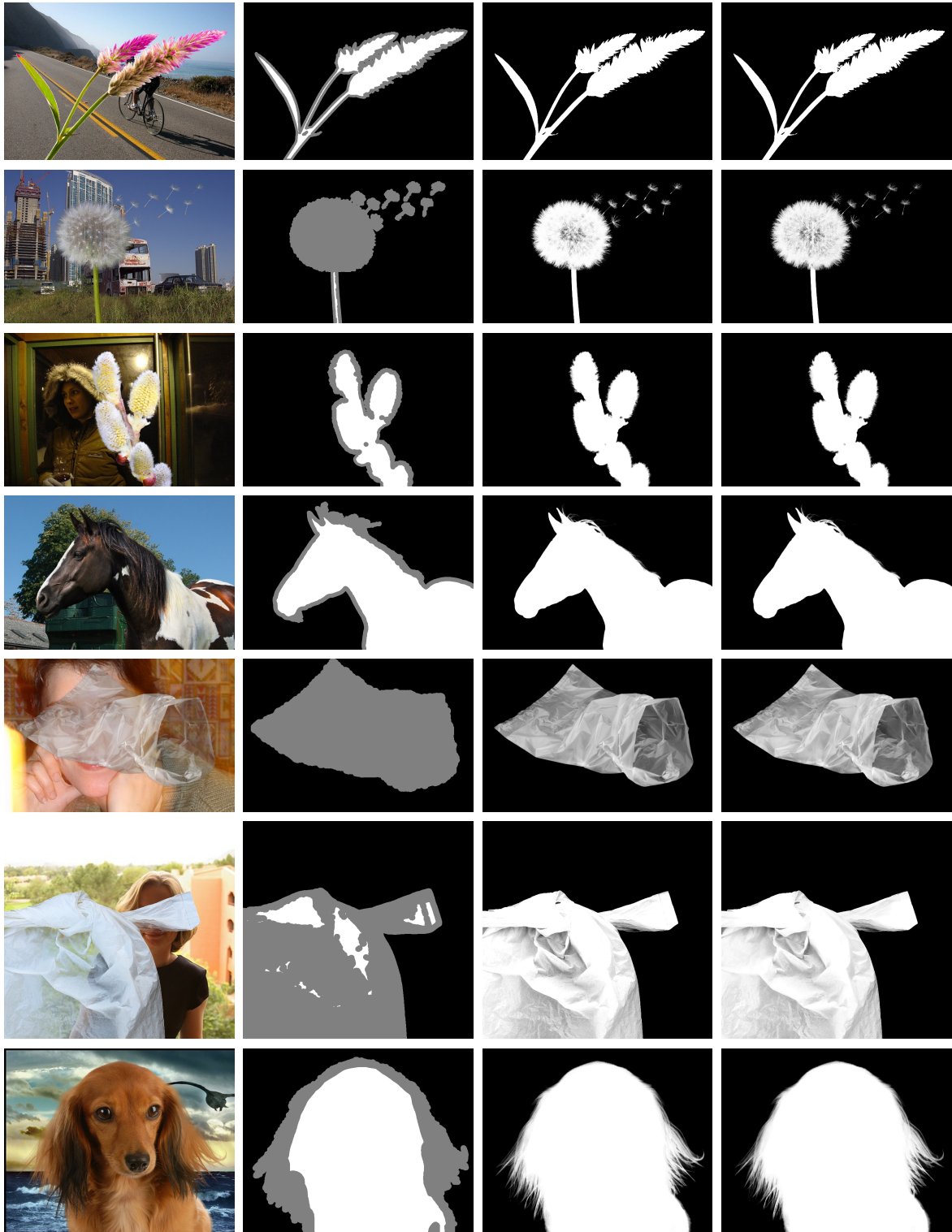


Figure 6: Qualitative results on the Adobe Composition-1K dataset.



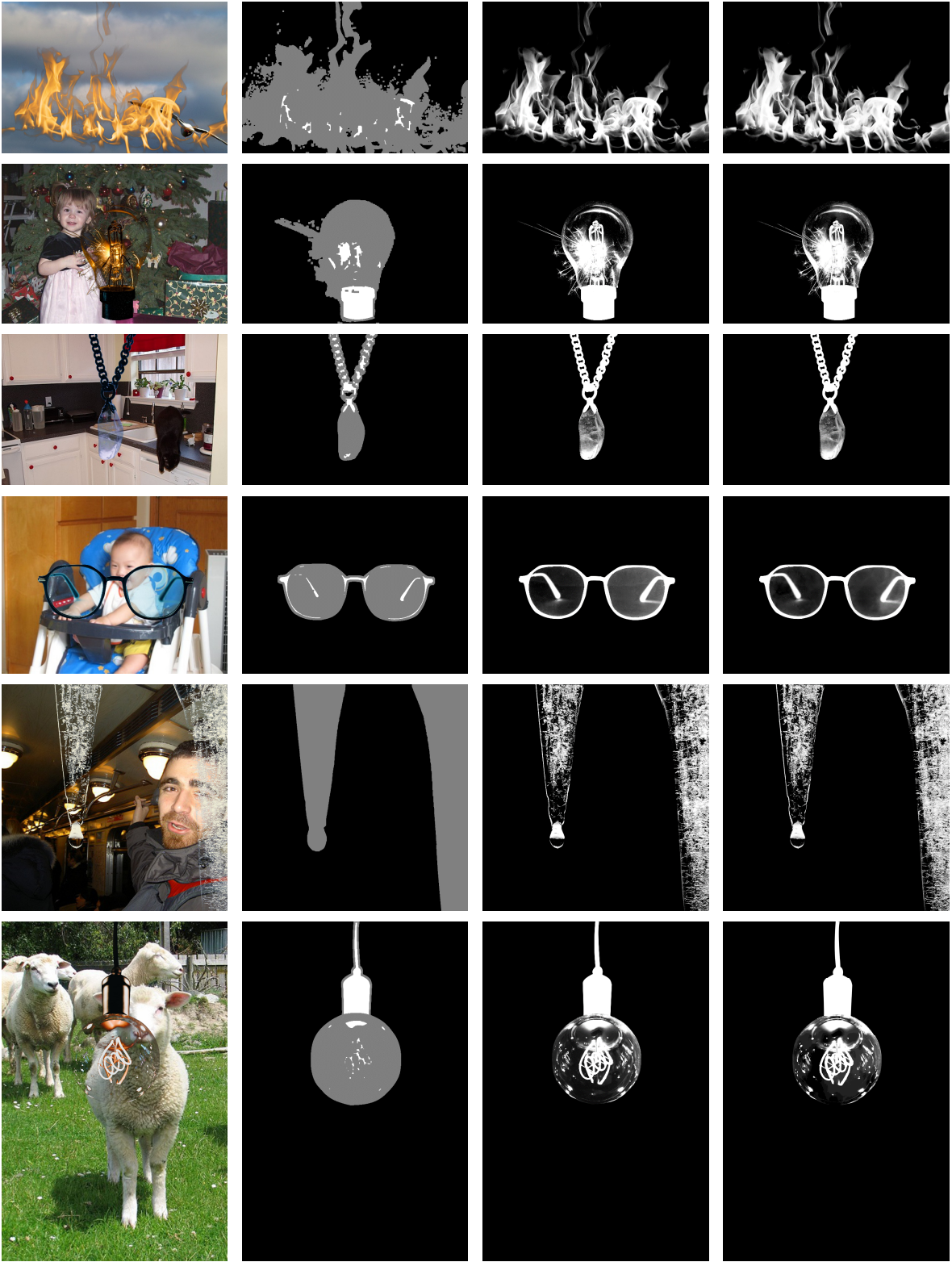
(a) Image

(b) Trimap

(c) Ground Truth

(d) AEMatter (Ours)

Figure 7: Qualitative results on the Distinction-646 dataset.



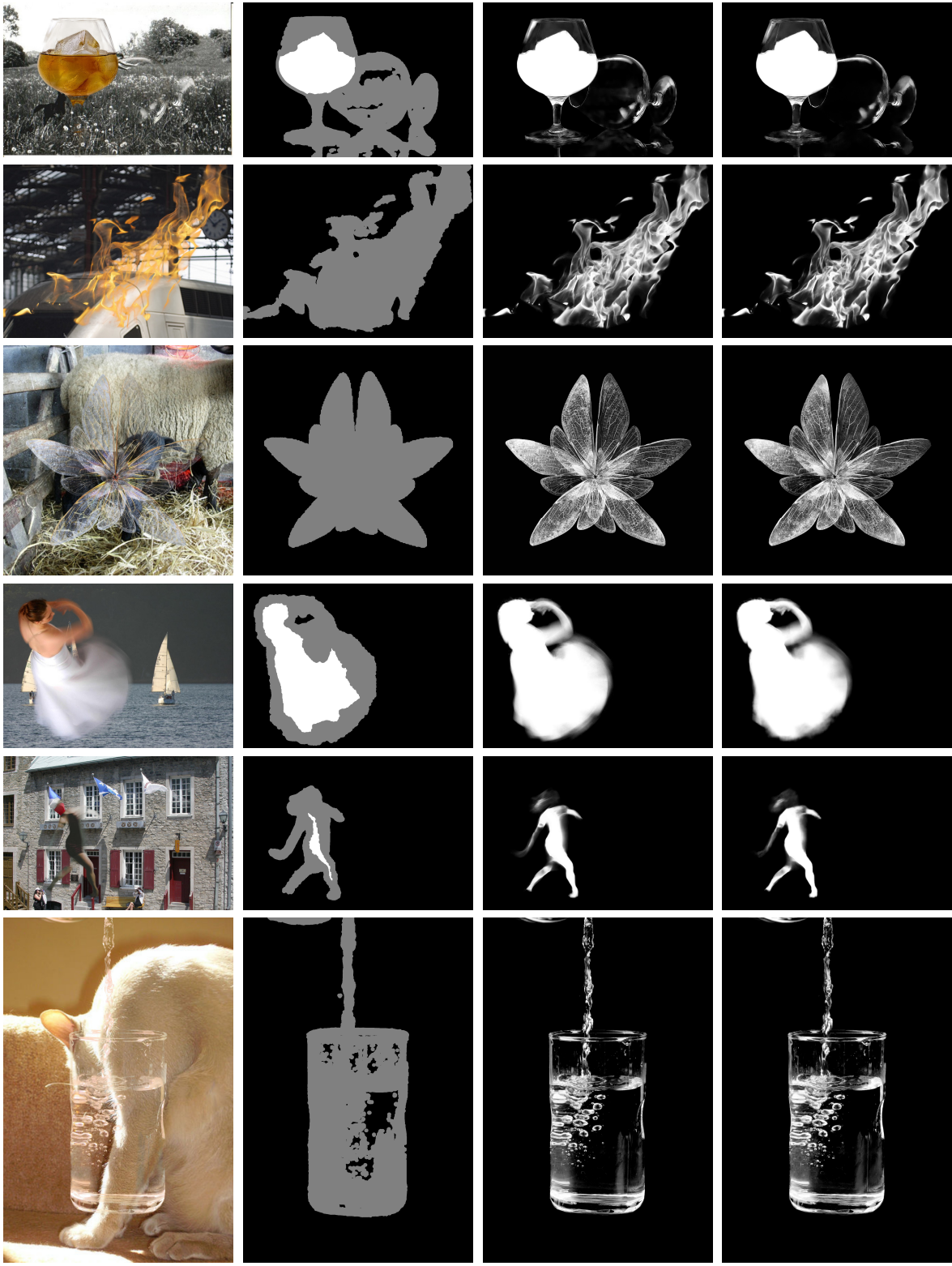
(a) Image

(b) Trimap

(c) Ground Truth

(d) AEMatter (Ours)

Figure 8: Qualitative results on the Transparent-460 dataset.



(a) Image

(b) Trimap

(c) Ground Truth

(d) AEMatter (Ours)

Figure 9: Qualitative results on the Semantic Image Matting dataset.

- [24] Dingzeyu Li, Qifeng Chen, and Chi-Keung Tang. Motion-Aware KNN Laplacian for Video Matting. In *ICCV*, 2013. [2](#)
- [25] Yaoyi Li and Hongtao Lu. Natural Image Matting via Guided Contextual Attention. In *AAAI*, 2020. [2](#), [3](#), [4](#), [7](#), [8](#), [10](#)
- [26] Liyuan Liu, Haoming Jiang, Pengcheng He, Weizhu Chen, Xiaodong Liu, Jianfeng Gao, and Jiawei Han. On the Variance of the Adaptive Learning Rate and Beyond. In *ICLR*, 2020. [6](#)
- [27] Yuhao Liu, Jiake Xie, Yu Qiao, Yong Tang, and Xin Yang. Prior-Induced Information Alignment for Image Matting. *TMM*, 24:2727–2738, 2022. [2](#)
- [28] Yuhao Liu, Jiake Xie, Xiao Shi, Yu Qiao, Yujie Huang, Yong Tang, and Xin Yang. Tripartite Information Mining and Integration for Image Matting. In *ICCV*, 2021. [3](#), [4](#), [7](#), [8](#), [10](#)
- [29] Ze Liu, Yutong Lin, Yue Cao, Han Hu, Yixuan Wei, Zheng Zhang, Stephen Lin, and Baining Guo. Swin Transformer: Hierarchical Vision Transformer using Shifted Windows. In *ICCV*, 2021. [3](#), [4](#), [5](#), [8](#), [9](#)
- [30] Liu, Qinglin and Xie, Haozhe and Zhang, Shengping and Zhong, Bineng and Ji, Rongrong. Long-Range Feature Propagating for Natural Image Matting. In *ACM MM*, 2021. [2](#), [3](#), [7](#), [8](#), [10](#)
- [31] Hao Lu, Yutong Dai, Chunhua Shen, and Songcen Xu. Indices Matter: Learning to Index for Deep Image Matting. In *ICCV*, 2019. [2](#), [3](#), [4](#), [7](#), [8](#), [10](#)
- [32] Wenjie Luo, Yujia Li, Raquel Urtasun, and Richard Zemel. Understanding the Effective Receptive Field in Deep Convolutional Neural Networks. *NIPS*, 29, 2016. [9](#)
- [33] Sebastian Lutz, Konstantinos Amplianitis, and Aljosa Smolic. AlphaGAN: Generative adversarial networks for natural image matting. In *BMVC*, 2018. [2](#)
- [34] GyuTae Park, SungJoon Son, JaeYoung Yoo, SeHo Kim, and Nojun Kwak. MatteFormer: Transformer-Based Image Matting via Prior-Tokens. In *CVPR*, 2022. [2](#), [3](#), [4](#), [5](#), [7](#), [8](#), [10](#)
- [35] Adam Paszke, Sam Gross, Francisco Massa, Adam Lerer, James Bradbury, Gregory Chanan, Trevor Killeen, Zeming Lin, Natalia Gimelshein, Luca Antiga, Alban Desmaison, Andreas Kopf, Edward Yang, Zachary DeVito, Martin Raison, Alykhan Tejani, Sasank Chilamkurthy, Benoit Steiner, Lu Fang, Junjie Bai, and Soumith Chintala. PyTorch: An Imperative Style, High-Performance Deep Learning Library. In *NeurIPS*, 2019. [6](#)
- [36] Siyuan Qiao, Huiyu Wang, Chenxi Liu, Wei Shen, and Alan Yuille. Weight standardization. *arXiv preprint arXiv:1903.10520*, 2019. [2](#)
- [37] Yu Qiao, Yuhao Liu, Xin Yang, Dongsheng Zhou, and Xiaopeng Wei. Attention-guided hierarchical structure aggregation for image matting. In *CVPR*, 2020. [2](#), [6](#)
- [38] Yu Qiao, Yuhao Liu, Xin Yang, Dongsheng Zhou, Mingliang Xu, Qiang Zhang, and Xiaopeng Wei. Attention-guided hierarchical structure aggregation for image matting. In *CVPR*, 2020. [10](#)
- [39] M.A. Ruzon and C. Tomasi. Alpha Estimation in Natural Images. In *CVPR*, 2000. [1](#), [2](#)
- [40] Mark Sandler, Andrew Howard, Menglong Zhu, Andrey Zhmoginov, and Liang-Chieh Chen. MobileNetV2: Inverted Residuals and Linear Bottlenecks. In *CVPR*, pages 4510–4520, 2018. [4](#)
- [41] Ehsan Shahrian, Deepu Rajan, Brian Price, and Scott Cohen. Improving Image Matting Using Comprehensive Sampling Sets. In *CVPR*, 2013. [2](#)
- [42] Jian Sun, Jiaya Jia, Chi-Keung Tang, and Heung-Yeung Shum. Poisson Matting. In *SIGGRAPH*, 2004. [2](#)
- [43] Yanan Sun, Chi-Keung Tang, and Yu-Wing Tai. Semantic image matting. In *CVPR*, 2021. [2](#), [4](#), [6](#), [7](#), [10](#)
- [44] Huan Tang, Yujie Huang, Ming’E Jing, Yibo Fan, and Xiaoyang Zeng. Very Deep Residual Network for Image Matting. In *ICIP*, 2019. [2](#)
- [45] Ashish Vaswani, Noam Shazeer, Niki Parmar, Jakob Uszkoreit, Llion Jones, Aidan N Gomez, Łukasz Kaiser, and Illia Polosukhin. Attention is all you need. *NIPS*, 30, 2017. [6](#), [8](#)
- [46] Jue Wang and M.F. Cohen. Optimized Color Sampling for Robust Matting. In *CVPR*, 2007. [1](#), [2](#)
- [47] Rui Wang, Jun Xie, Jiacheng Han, and Dezhen Qi. Improving Deep Image Matting Via Local Smoothness Assumption. *arXiv preprint arXiv:2112.13809*, 2021. [2](#)
- [48] Rui Wang, Jun Xie, Jiacheng Han, and Dezhen Qi. Improving deep image matting via local smoothness assumption. In *ICME*, 2022. [4](#), [7](#)
- [49] Tiantian Wang, Sifei Liu, Yapeng Tian, Kai Li, and Ming-Hsuan Yang. Video Matting via Consistency-Regularized Graph Neural Networks. In *ICCV*, 2021. [1](#)
- [50] Yuxin Wu and Kaiming He. Group normalization. In *ECCV*, 2018. [2](#)
- [51] Enze Xie, Wenhai Wang, Zhiding Yu, Anima Anandkumar, Jose M Alvarez, and Ping Luo. SegFormer: Simple and Efficient Design for Semantic Segmentation with Transformers. In *NeurIPS*, 2021. [3](#)
- [52] Ning Xu, Brian Price, Scott Cohen, and Thomas Huang. Deep Image Matting. In *CVPR*, 2017. [2](#), [6](#), [7](#), [8](#), [10](#)
- [53] Haichao Yu, Ning Xu, Zilong Huang, Yuqian Zhou, and Humphrey Shi. High-Resolution Deep Image Matting. In *AAAI*, 2021. [2](#), [3](#)
- [54] Qihang Yu, Jianming Zhang, He Zhang, Yilin Wang, Zhe Lin, Ning Xu, Yutong Bai, and Alan Yuille. Mask Guided Matting via Progressive Refinement Network. In *CVPR*, 2021. [2](#), [3](#), [8](#), [9](#)
- [55] Zijian Yu, Xuhui Li, Huijuan Huang, Wen Zheng, and Li Chen. Cascade Image Matting With Deformable Graph Refinement. In *ICCV*, 2021. [3](#)
- [56] Hengshuang Zhao, Jianping Shi, Xiaojuan Qi, Xiaogang Wang, and Jiaya Jia. Pyramid scene parsing network. In *CVPR*, 2017. [2](#)